ULTRAVIOLET ASTRONOMY IN THE XXI CENTURY
MEETING IN BASQUE COUNTRY UNIVERSITY,
VITORIA-GASTEIZ (SPAIN)
3rd- 7th October 2022

Hot atomic coronas at terrestrial planets - evidence in the UV observations

Valery I. Shematovich
Institute of Astronomy RAS, 48 Pyatnitskaya str., Moscow 119017, Russia.
e-mail: shematov@inasan.ru

Hot atomic coronas at terrestrial planets

Outline:

- **Thermal and hot (suprathermal) atoms in the planetary coronas**
- **Modeling of suprathermal atoms**
- **Hot oxygen corona at Earth**
- **Hot hydrogen and oxygen coronas at Mars**
- **Hot exoplanets**
- **Conclusions**

UV observations of hot hydrogen and oxygen coronas of the terrestrial planets

The uppermost layer of a planetary atmosphere, where the density of neutral particles is vanishingly low, is commonly called the exosphere or the planetary corona and is populated mainly by H, C, N and O atoms for terrestrial planets.
Current theories of atomic coronas are based mainly on space observations of exospheric emission features in the Ly-α line for hydrogen and 130.4 and 135.6 nm atomic lines for oxygen.

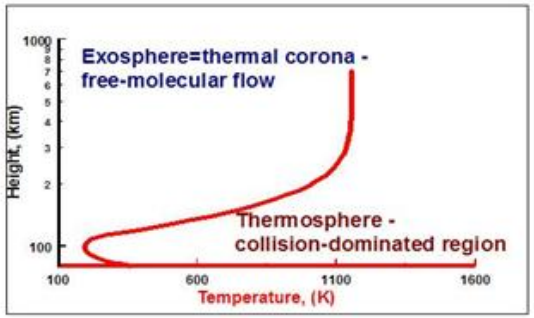

Measurements reveal that hot atomic corona contain both a fraction of thermal neutral particles with a mean kinetic energy corresponding to the exospheric temperature and a fraction of hot neutral particles with mean kinetic energy much higher than the exospheric temperature for many types of background atmospheres – N2-O2 for the Earth; CO2 – for Mars; O2, H2O for icy moons such as Europa and Ganymede.

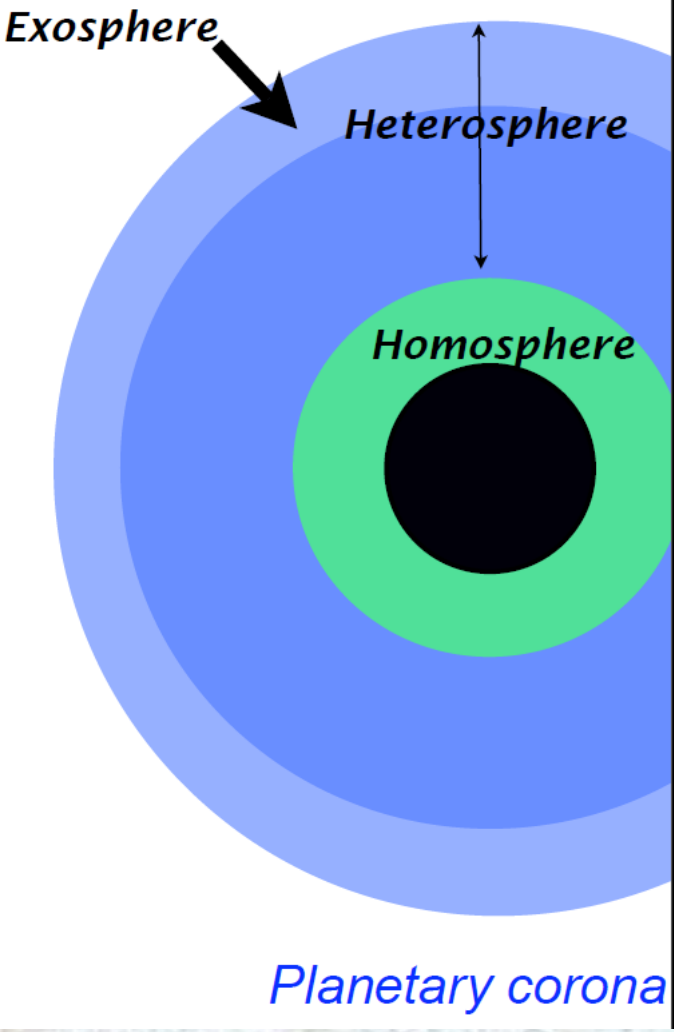

Hot planetary coronas

Hot and thermal hydrogen corona at Venus discovered by Mariner 5 (Anderson, 1976). The observed hydrogen Ly-α emission was fitted to thermal fraction at 275 K (blue symbols) and to a non-thermal fraction at 1020 K (red symbols).

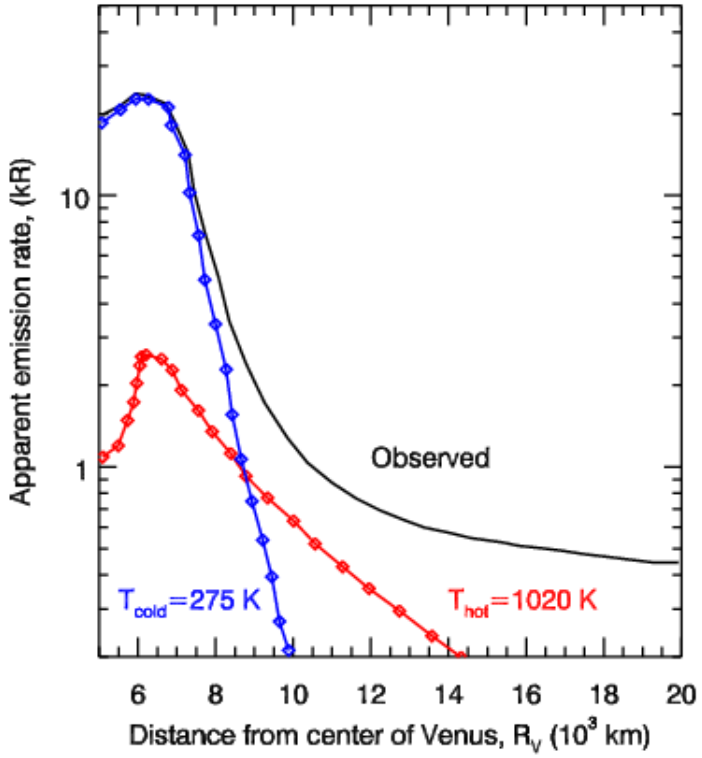

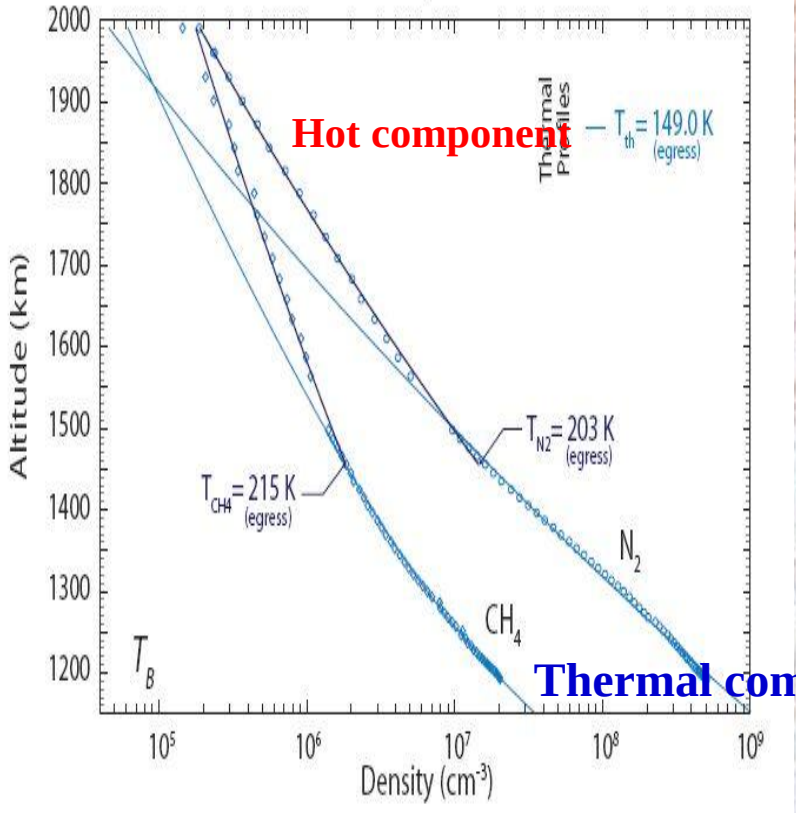

Cassini at Titan - INMS data: Fit of the Tb INMS data using a thermal exospheric model (H. Waite et al., 2006) - First direct measurement of hot corona!!!

Hot planetary coronas

Cassini at Titan - INMS data: Fit of the Tb INMS data using a thermal exospheric model (H. Waite et al., 2006) - First direct measurement of hot corona!!!

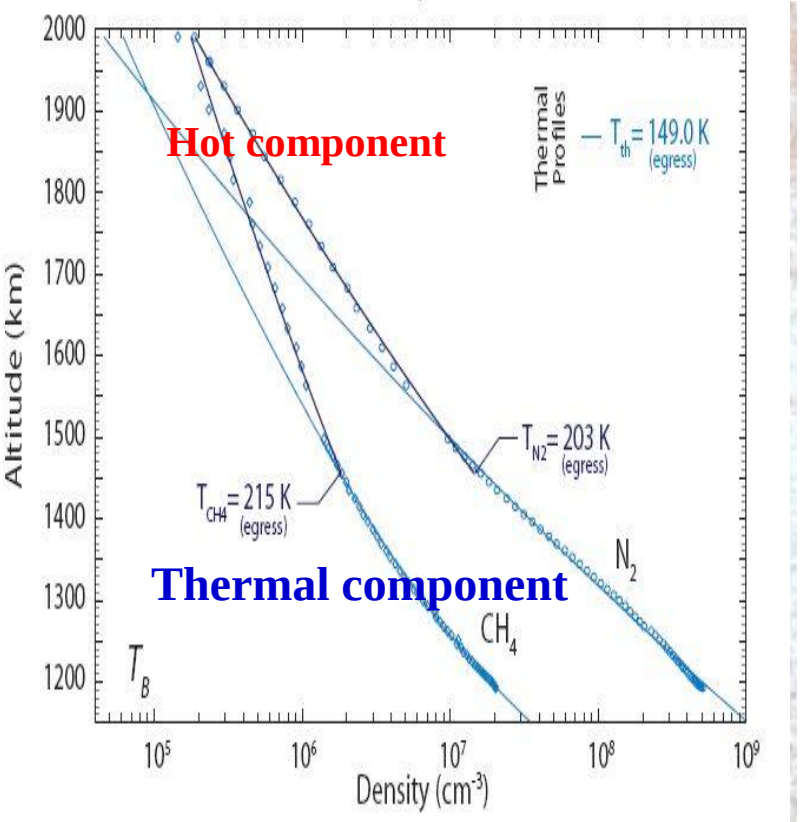

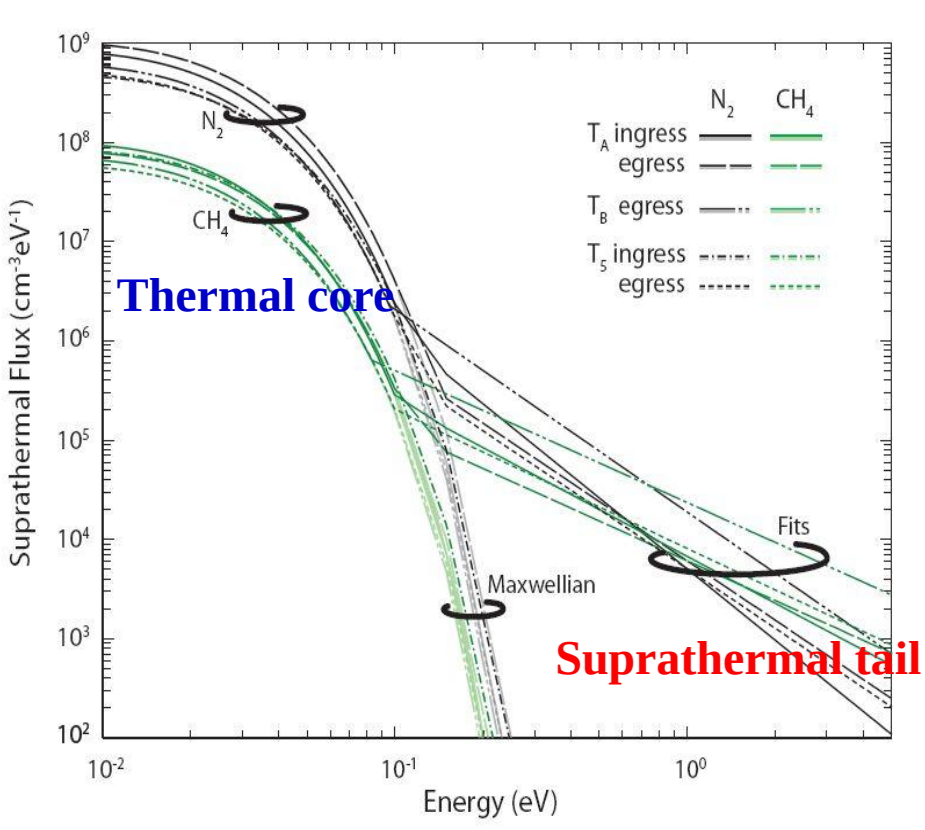

Cassini at Titan - INMS data: Fits of the energy distribution functions for N2 and CH4 (H. Waite et al., 2006)

Introduction/motivation: *non-thermal particles*

Non-thermal particles – particles with an excess of the kinetic and/or inner energy,
-Thermal particles – ones with kinetic energies E ~ kT;
-Non-thermal particles:
-Suprathermal particles – ones with kinetic energies E ~ 5—10 kT;
-Superthermal particles – ones with kinetic energies E ~> 100 kT.

-Suprathermal particles are described by nonlinear kinetic Boltzmann equation –no small parameter by energy kT/E ~ 0.1 -- 0.2.

Earth's upper atmosphere at 500 km

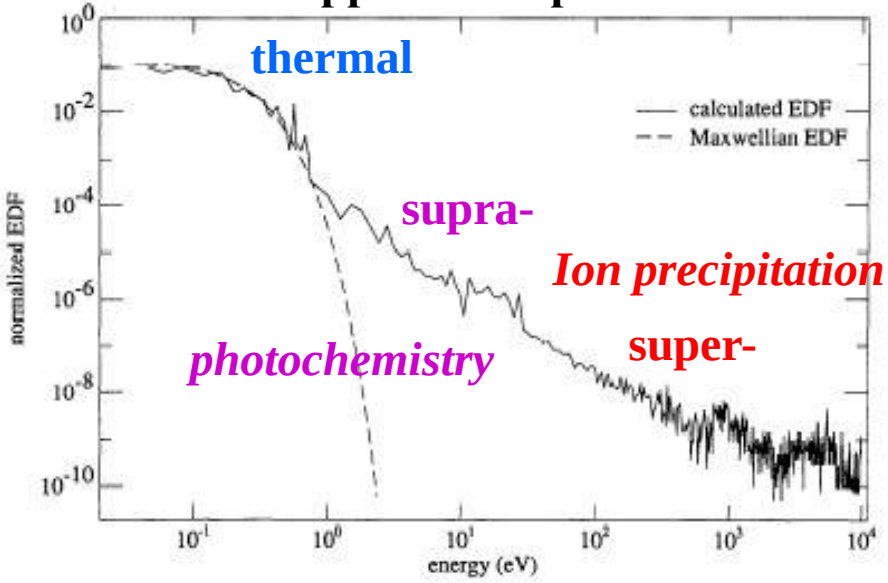

Figure 1. Energy distribution functions (EDF) for atomic oxygen in the transition region at 500 km. The solid line shows the calculated distribution and the dashed line represents the local Maxwellian distribution function (T = 1170 K). **From (Shematovich et al., 1994; Bisikalo et al., 1995)**

Non-thermal atoms and molecules are produced in various nonthermal processes:

- ✓ **charge exchange;**
- ✓ **dissociative recombination of ions;**
- ✓ **impact dissociation by photons and charged particles;**
- ✓ **exothermic ion-neutral chemical reactions;**
- ✓ **ion precipitation, sputtering or knock-on;**
- ✓ **chemical exchange through the atmosphere-surface interface.**

Suprathermal particles: *kinetics*

Distribution of suprathermal atoms in the atmospheric rarefied gas is evaluated through the solution of Boltzmann-type kinetic equations with the source terms

$$\frac{\partial}{\partial t}F_i + \vec{c}\,\frac{\partial}{\partial \vec{r}}F_i + \vec{g}\,\frac{\partial}{\partial \vec{c}}F_i = \sum_{\beta} Q_i^{\beta} + \sum_j \sum_{\alpha} J_{\alpha}(F_i, F_j)$$

$$F_i(t = t_0) = F_i^{(0)}(\vec{r}, \vec{c}), \quad F_i(\vec{r} \in \Gamma(G)) = F_i^{(1)}(t, \vec{c})$$

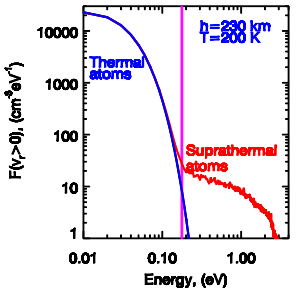

Here Q_α are the source functions of the fresh suprathermals and $J_\alpha(F_i,F_j)$ – integral terms for collisions with the ambient atmospheric gas.

Collision-free region $J_\alpha << Q_\alpha$ *Linear Boltzmann eq.*

Transition region $J_\alpha \sim Q_\alpha$ *Nonlinear Boltzmann eq.*

Collision-dominated region $J_\alpha >> Q_\alpha$ *HD equations*

This system of kinetic equations for suprathermal particles is solved using the stochastic modeling (Marov et al., SSRs, 1996) with kinetic Monte Carlo method.

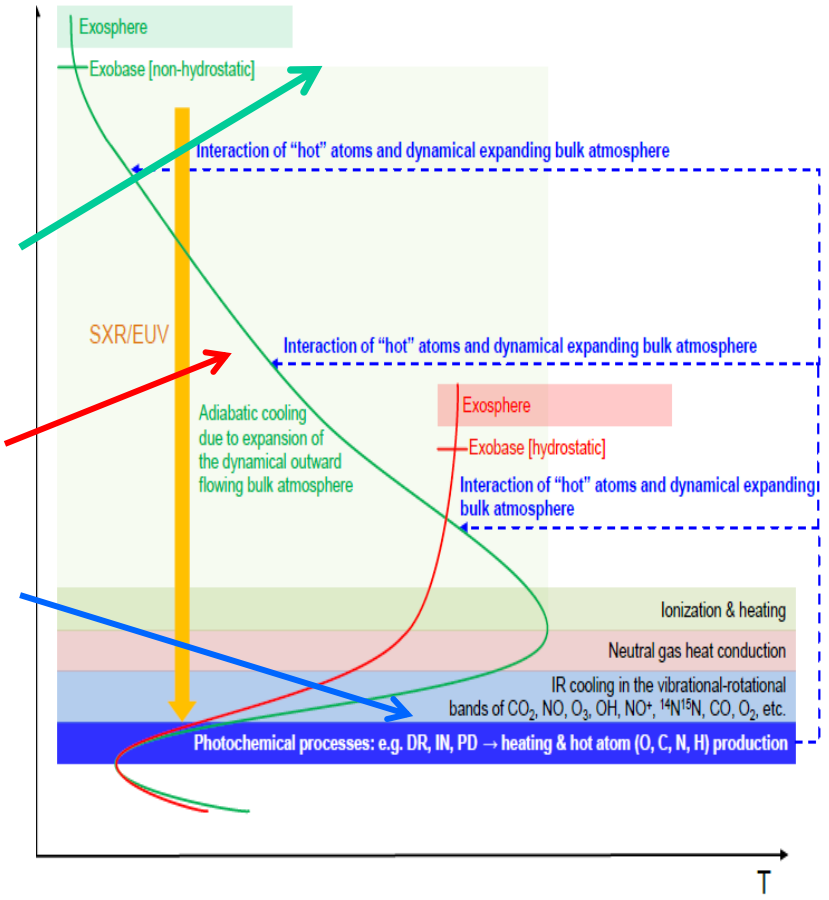

Kinetic Monte Carlo modeling

$$\{a^{\alpha}\}_{(M^{\alpha})} \to \{a_i^{\alpha}\}_{(M^{\alpha},N)}, \quad N = \sum_{\alpha} N^{\alpha}$$

$$\vec{C} = \bigcup_{\alpha} \vec{C}^{\alpha}, \vec{C}^{\alpha} = \bigcup_{i} \vec{c}_i^{\alpha} = \{N^{\alpha}, \vec{c}_1^{\alpha}, \ldots, \vec{c}_{N^{\alpha}}^{\alpha}\}$$

$$\vec{C} \to \vec{C}' \quad : \vec{c}_i^{\alpha}, \vec{c}_j^{\beta} \to \vec{c}_{i'}^{\alpha(r)}, \vec{c}_{j'}^{\beta(r)}$$

a) rarefied atmospheric gas is replaced by finite system of modeling particles;

b) distribution function by the system state vector;

c) collisions by the jump-like transitions between the system states.

a) approximation of a set of the atmospheric gas by the system of finite number of modeling particles (mathematical model);

b) selection of a random process which describes the evolution of the numerical system due to the chemical reactions:

$$m: \alpha_i(\boldsymbol{c}_i, \boldsymbol{z}_i) + \alpha_j(\boldsymbol{c}_j, \boldsymbol{z}_j) \to \alpha_k(\boldsymbol{c}_k', \boldsymbol{z}_k) + \alpha_l(\boldsymbol{c}_l', \boldsymbol{z}_l);$$

c) probabilistic description of the numerical model - stochastic master equation which approaches the kinetic system under study. Reaction probabilities are determined by the scattering functions for chemical reactions:

$$g_{ij} d\sigma_m = |\boldsymbol{c}_i - \boldsymbol{c}_j| d\sigma_m(|\boldsymbol{c}_i - \boldsymbol{c}_j|, \Omega) d\Omega, \quad \sigma_m = \sigma_m^{(el)} + \sigma_m^{(in)} + \sigma_m^{(r)}$$

d) Algorithmic realization of the model is an analogue Monte Carlo procedure for solution of the linear (!!!) stochastic master equation. Therefore, efficiency of algorithm and the limits of its applicability can be directly estimated.

-Shematovich & Marov, Uspiekhi – Physics, 2018; Shematovich, Russian Chem. Reviews, 2019.

Suprathermal oxygen in the Earth's atmosphere: *First indirect UV observations*

Satellite observations of the 73.3 nm O+ emission line with the Fabri-Pierrot interferometer showed the line broadening corresponding to the effective temperature of ~ 4300 K (Yee et al., JGR, 1980)

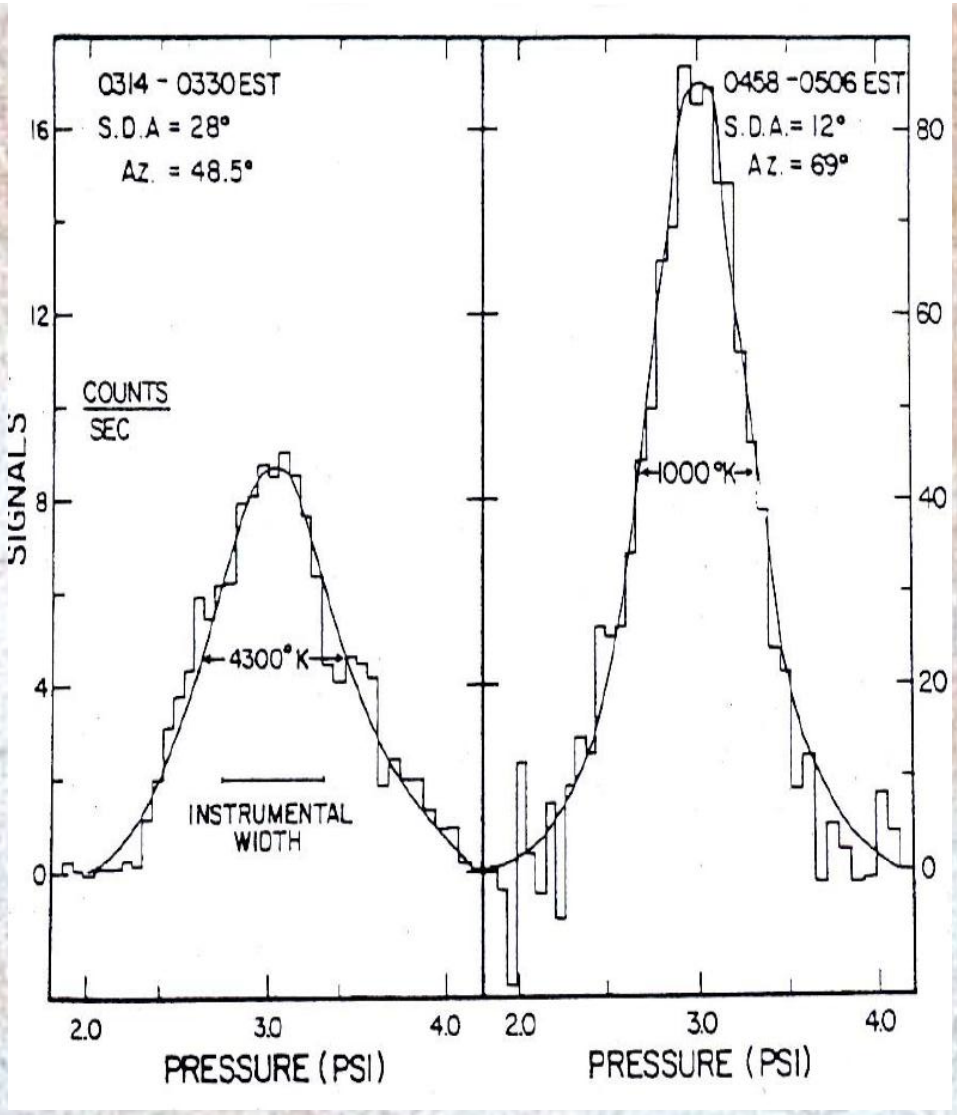

Hot oxygen geocorona: *sources*

- **O_2^+dissociative recombination (*Kella et al. 1997*)**

$$O_2^+ + e \rightarrow \begin{cases} O(^3P) + O(^3P) + 6.99 \ eV \\ O(^3P) + O(^1D) + 5.02 \ eV \\ O(^1D) + O(^1D) + 3.06 \ eV \\ O(^1D) + O(^1S) + 0.84 \ eV \end{cases}$$

- **Exothermic chemistry (~30 reactions; *Hickey et al., JGR, 1995*)**
- **O+ ion precipitation from ring current (strongly disturbed geomagnetic conditions)**

Hot oxygen geocorona: *energy distribution functions*

Hot thermal O ~ 1110 K;

Hot non-thermal O ~ 4500 K (*Shematovich et al., 1994, 2005; Bisikalo et al., 1995; Hubert et al., 2015*).

This difference in scale heights is seen in the observations, see e.g., *Hedin (1989)*.

Exothermic photochemistry

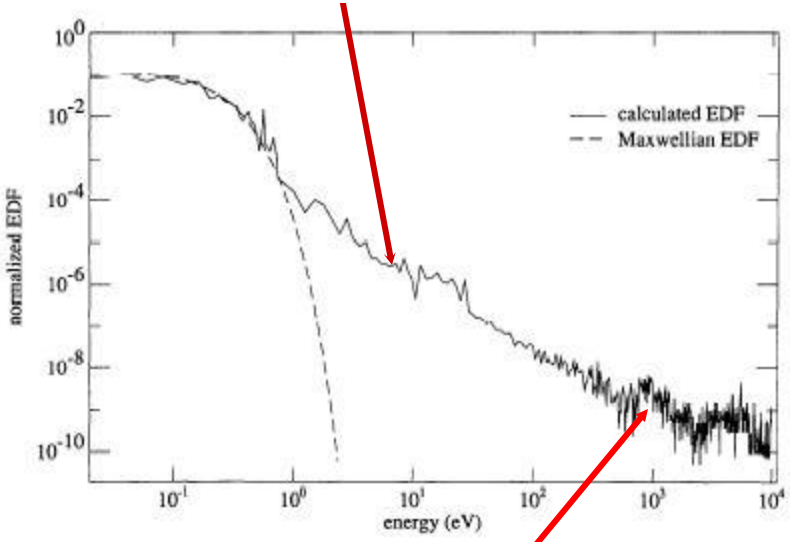

Figure 1. Energy distribution functions (EDF) for atomic oxygen in the transition region at 500 km. The solid line shows the calculated distribution and the dashed line represents the local Maxwellian distribution function (T = 1170 K).

H+, O+ precipitation

Non-thermal hot O

Thermal hot O

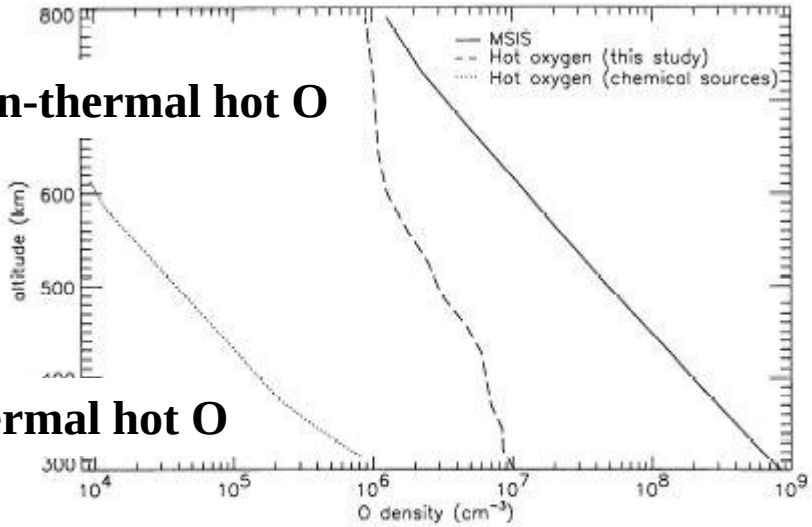

Figure 4. Vertical profiles of the hot and thermal fractions of atomic oxygen in the transition region. The dashed line is the hot fraction and the solid line is the MSIS density profile of thermal oxygen. For comparison, the hot O density produced by chemical sources (paper 1) (dotted line) is also presented.

Oxygen geocorona: *O height profiles and observations of UV emission excess*

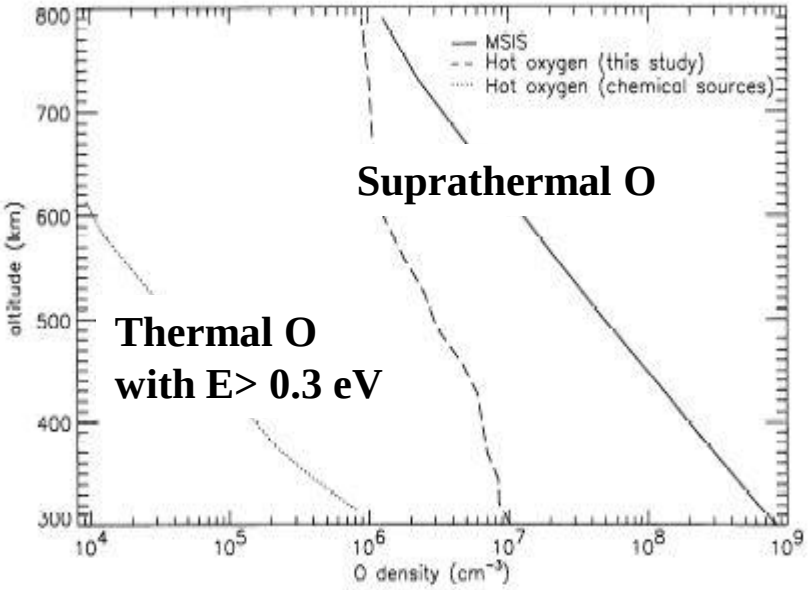

Figure 4. Vertical profiles of the hot and thermal fractions of atomic oxygen in the transition region. The dashed line is the hot fraction and the solid line is the MSIS density profile of thermal oxygen. For comparison, the hot O density produced by chemical sources (paper 1) (dotted line) is also presented.

Thermal O ~ 1110 K;
Suprathermal O ~ 4500 K.
This difference in scale heights is seen in the observations, see e.g., Hedin (1989). Figures from Shematovich et al., JGR, 1994; Bisikalo et al., 1995).

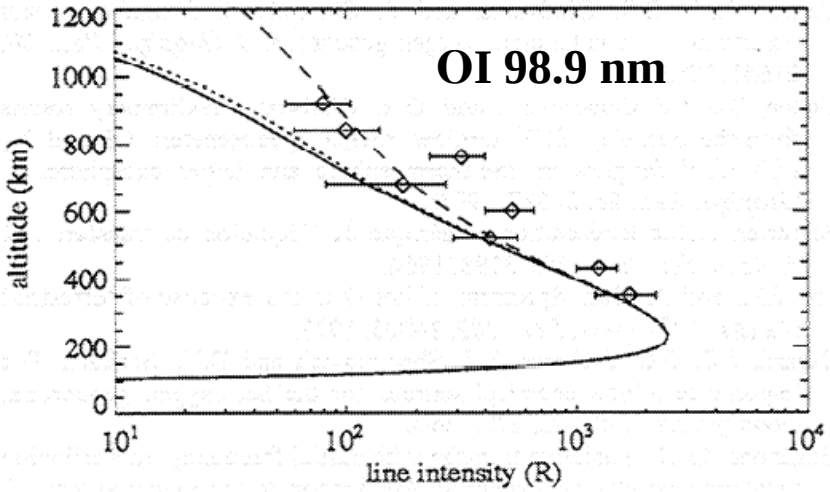

Figure 4. Intensity profile of the OI 989 Å multiplet measured by *Cotton et al.* [1993a] under a 97.5° zenith angle view direction (diamonds with error bars) and calculated with the radiative transfer model for the day of the measurement under three different hypotheses: MSIS atmosphere only (solid lines), including the calculated nonthermal $O(^3P)$ with total O density from the MSIS model (dotted lines) and including the nonthermal oxygen concentration used by *Cotton et al.* [1993a] (dashed lines).

Intensity excess of OI 98.9 nm multiplet emission in the Earth's upper atmosphere:
thermal distribution – solid line;
-with the suprathermal O atoms – dashed line;
-circles represent the data of rocket measurements (Hubert et al., JGR 1999; 2015).

Hot atomic coronae at Mars: *MAVEN/IUVS data*

Currently, MAVEN is the best observer of atmospheric escape anywhere in the Solar system. Consequently, Mars serves as a natural laboratory for understanding the evolution of the terrestrial planet atmospheres. First observations of the extended upper atmosphere surrounding Mars with the Imaging UV Spectrograph (IUVS) instrument. The image shows the planet from an altitude of 36,500 km in three UV wavelength bands:

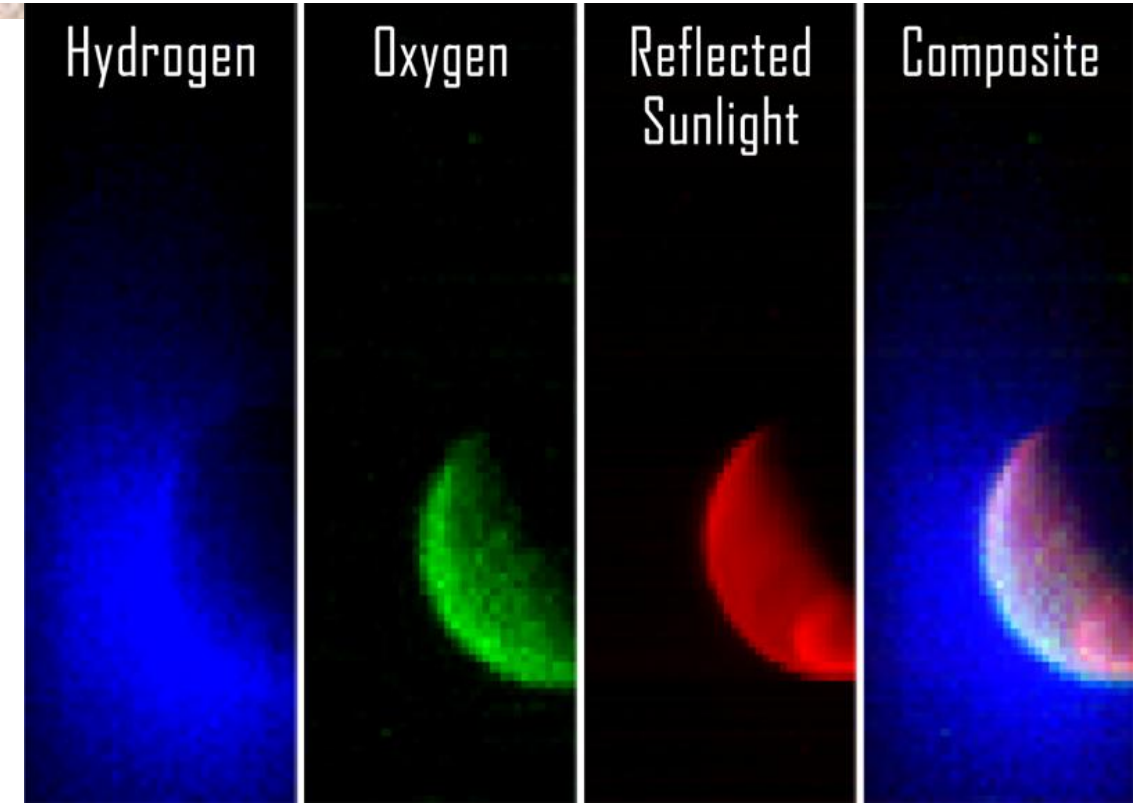

Credits: NASA/MAVEN/University of Colorado

-Blue shows the UV light from the sun scattered from atomic hydrogen gas in an extended cloud that goes to thousands of kilometers above the planet's surface.

-Green shows a different UV wavelength light that is primarily sunlight reflected off of atomic oxygen, showing the smaller oxygen cloud.

- Red shows UV sunlight reflected from the planet's surface; the bright spot in the lower right is light reflected either from polar ice or clouds.

Hot oxygen corona at Mars: *photochemical sources*

Production rates of suprathermal oxygen atoms due to the photochemical sources with the main source – dissociative recombination of O2+ ion (Groeller et al., PSS, 2014):

$$O_2^+ + e \rightarrow$$

$$\rightarrow \begin{cases} O(^3P) + O(^3P) + 6.99 \quad eV \\ O(^3P) + O(^1D) + 5.02 \quad eV \\ O(^1D) + O(^1D) + 3.06 \quad eV \\ O(^1D) + O(^1S) + 0.84 \quad eV \end{cases}$$

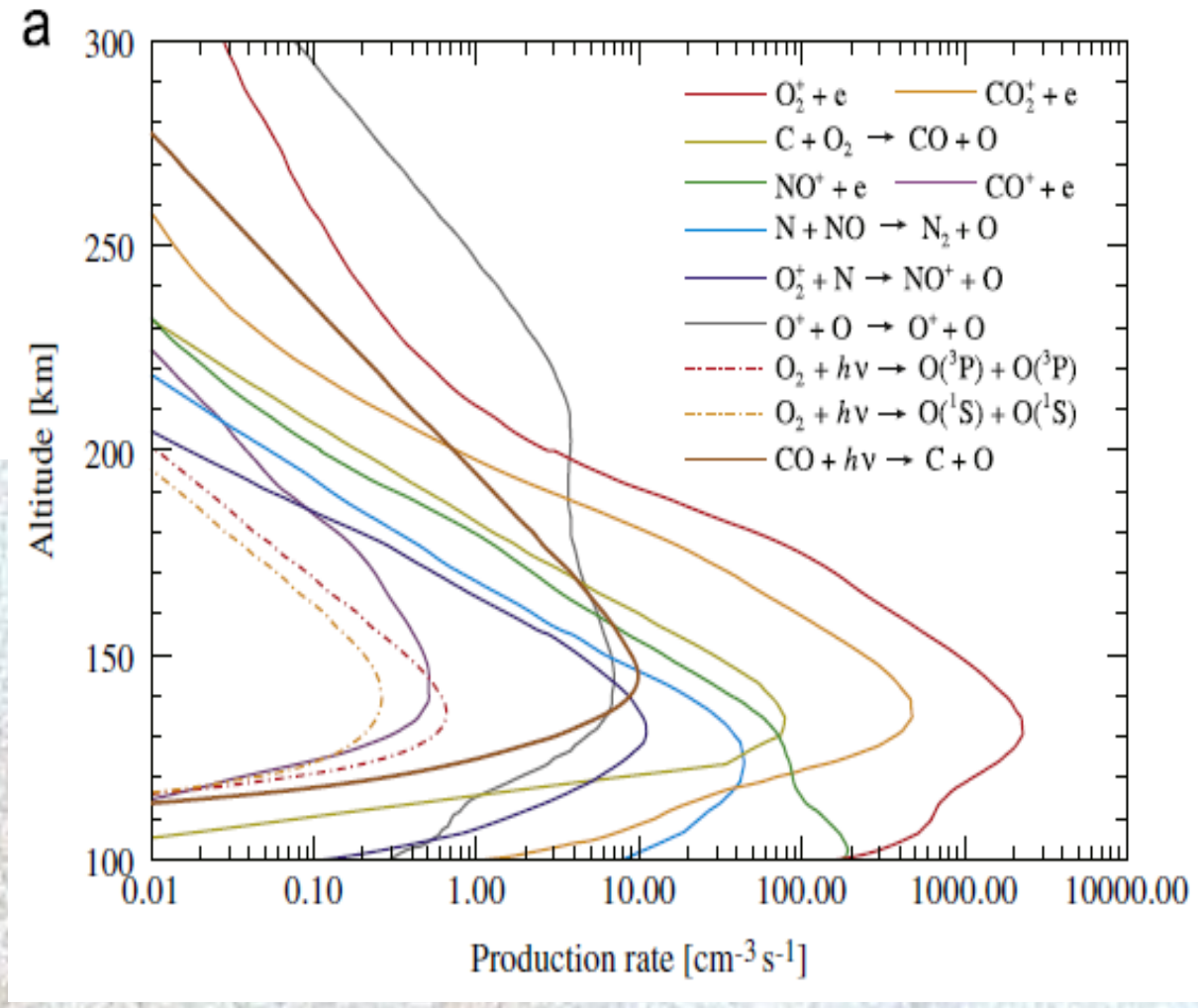

Hot oxygen corona at Mars: *photochemical sources*

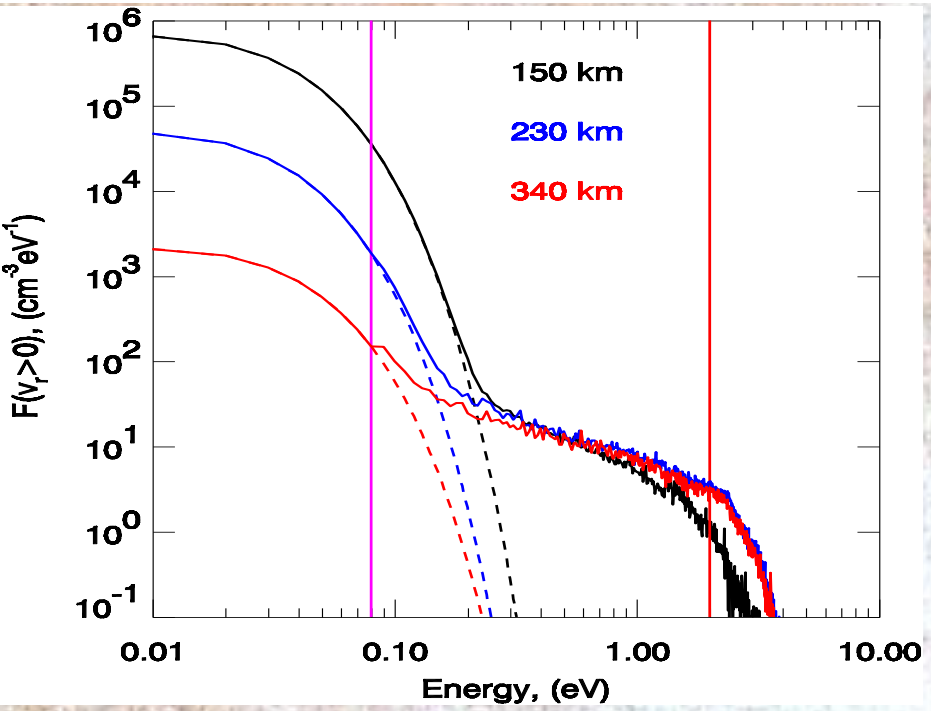

Calculated EDFs – solid lines;
Locally equilibrium EDFs – dashed lines;
Left vertical line shows the range of suprathermal energies;
Right vertical line – escape energy for O atoms.
Calculated escape flux ~ (0.5 – 1.)×10^7 cm^{-2} s^{-1}(Krestyanikova& Shematovich, 2005; Groeller et al., 2014).

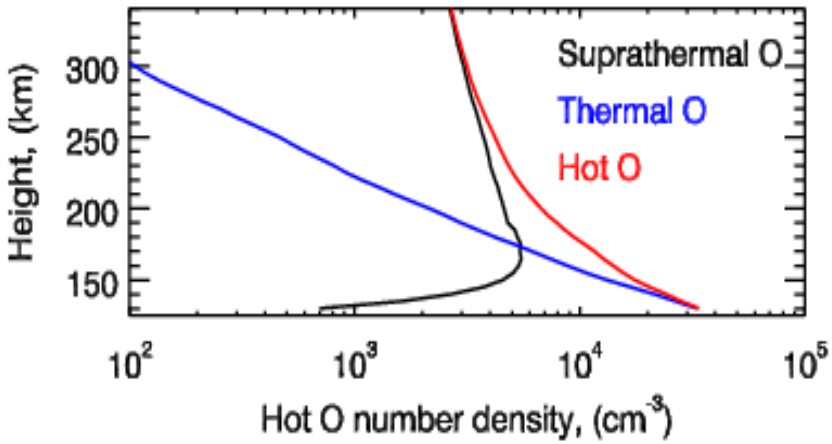

Hot oxygen corona at Mars:
Height distributions of hot thermal (blue line) and non-thermal (black line) oxygen in the Mars upper atmosphere are shown in top panel. The total distribution is shown by red line calculated by the kinetic MC model by Krestyanikova & Shematovich (2005, 2006).

Hot oxygen corona at Mars: *evidence in UV observations*

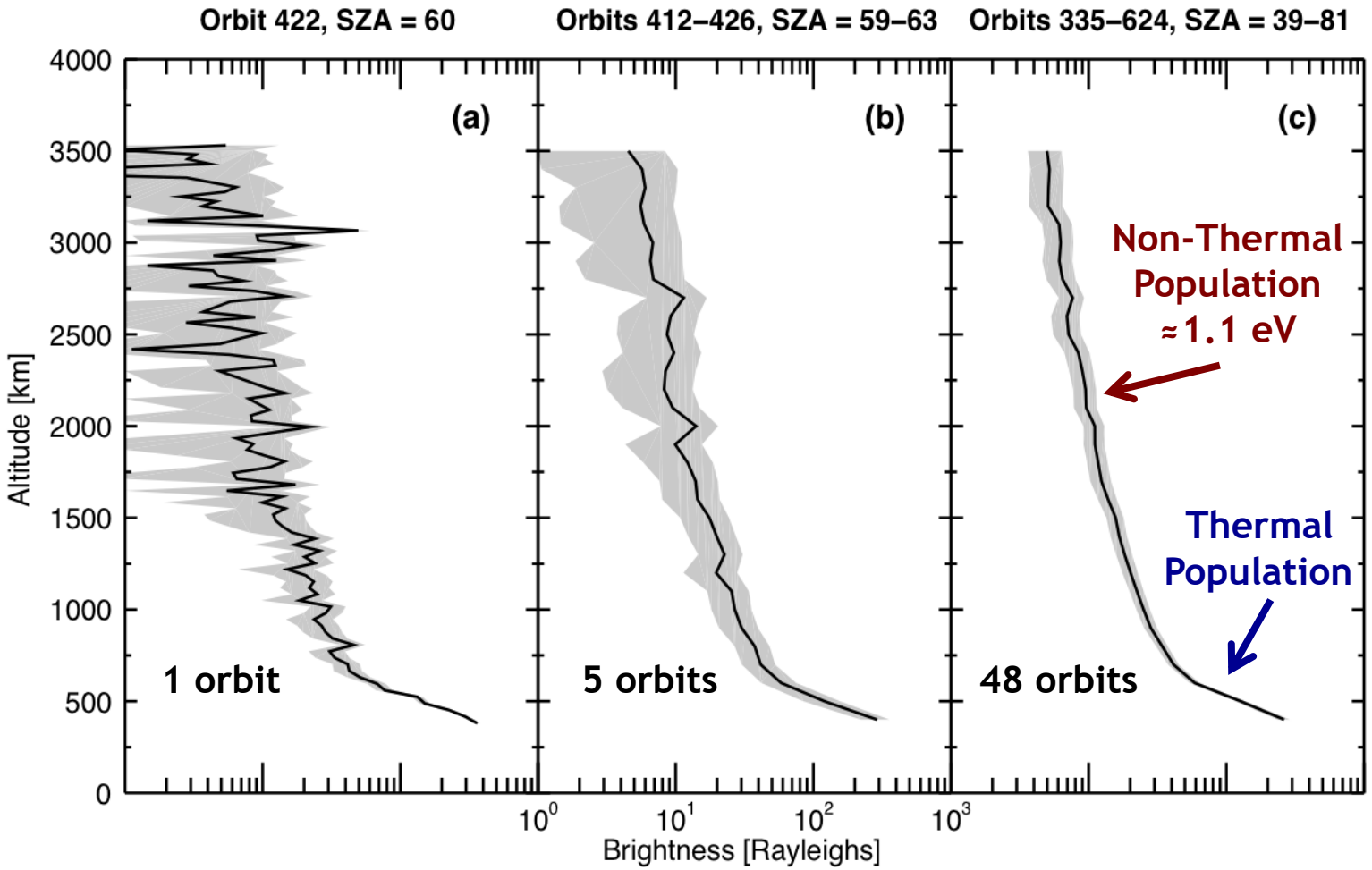

O 130.4 nm Brightness Profiles *(Deighan et al. 2016)*

Proton aurora at Mars: *H Ly-α emission*

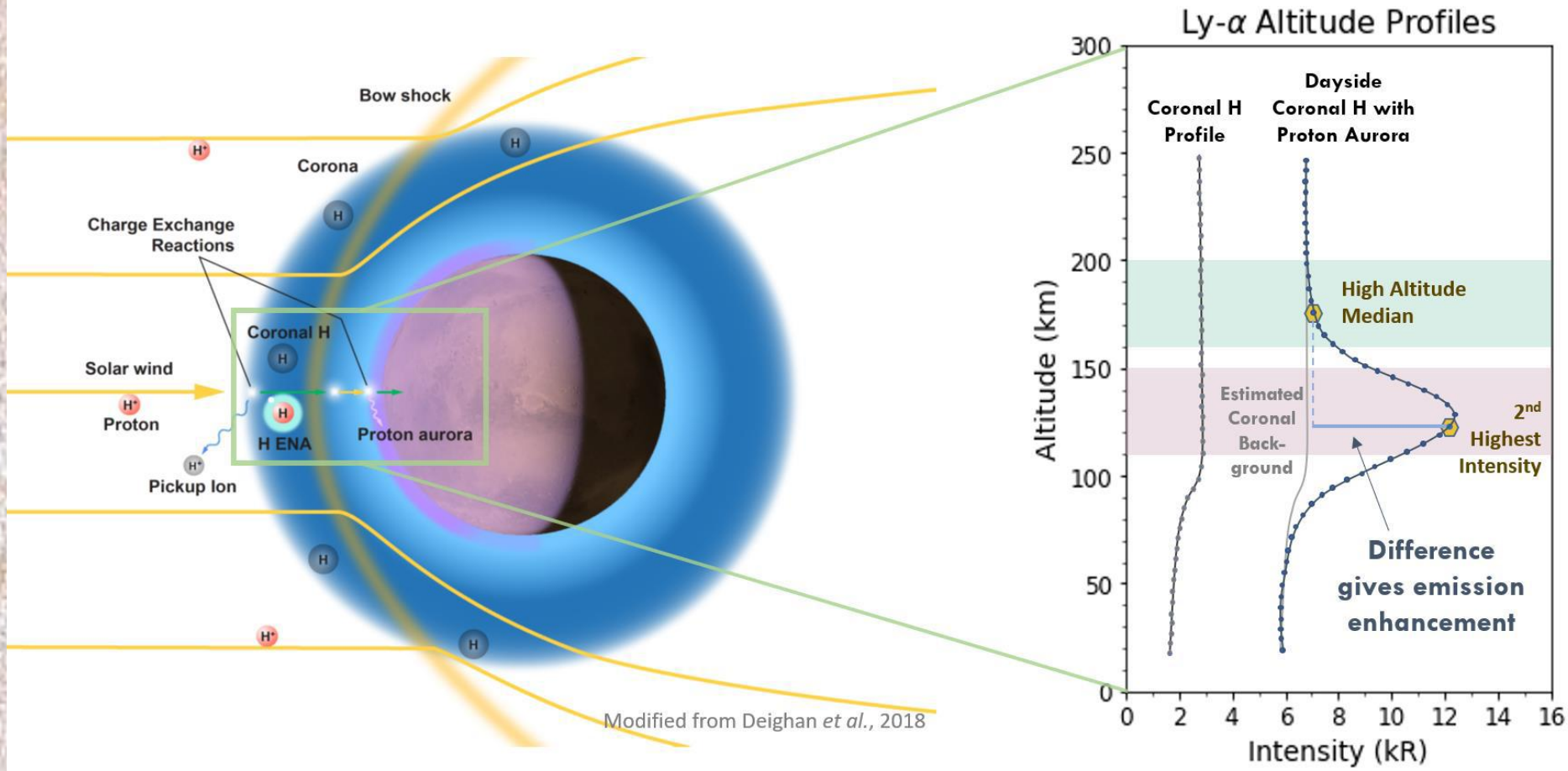

Example H Lyman-α altitude profile for coronal H (dark grey) and profile with proton aurora detection (blue) including a heuristic estimated coronal background profile for reference (light grey) (note that the background coronal profile is not distinguishable from proton aurora in the data). emission enhancement differences above a predetermined threshold (described in Figure 2) are considered detections (Hughes et al., JGR, 2019).

Proton aurora at Mars: *additional source of suprathermal H and O atoms due to the ENA-H precipitation*

Interactions of precipitating energetic H+ and H with the ambient atmosphere include: (i) the momentum and energy transfer in elastic and inelastic collisions; (ii) ionization of target atmospheric molecules/atoms, and (iii) charge transfer and electron capture collisions.

$$H^+(H) + M \rightarrow (i)\ H^+_{f'}(H_{f'}) + M^*; (ii)\ H^+_{f'}(H_{f'}) + M^+ + e; (iii)\ H_{f'}(H^+_{f'}) + M^+(M) + (e)$$

The energy deposition rate of H/H^+ flux is determined by the cross sections of the collisions with the ambient gas. The energy lost by the H/H^+ in a collision is determined by the scattering angle χ

$$\Delta E = E_{H/H+} \times \left(\frac{2 m_M m_{H/H+}}{(m_M + m_{H/H+})^2} \right) \times (1 - \cos\chi)$$

where $E_{H/H+}$ is the initial energy of the impacting proton or hydrogen atom.

The momentum transfer collisions of high-energy H/H^+ flux with the ambient atmospheric H and O atoms are the additional source of hot H and O in the upper atmosphere of Mars (Shematovich, 2013;2017)

$$Q_{Hh,Oh} : H^+[H](E) + H_{thermal}, O_{thermal} \rightarrow H^+[H](E' < E) + H_{hot}, O_{hot}(\Delta E)$$

This source was taken into account in the kinetic Boltzmann equation for hot H and O

$$\mathbf{v} \frac{\partial}{\partial \mathbf{r}} f_{Hh,Oh} + \mathbf{g} \frac{\partial}{\partial \mathbf{v}} f_{Hh,Oh} = Q_{Hh,Oh}(\mathbf{v}) + \sum_{M = H, O, N_2, CO_2} J_{mt}(f_{Hh,Oh}, f_M)$$

and this equation was solved using the kinetic Monte Carlo model (Shematovich, 2004).

Proton auroral events at Mars: *up- and downward Oh fluxes*

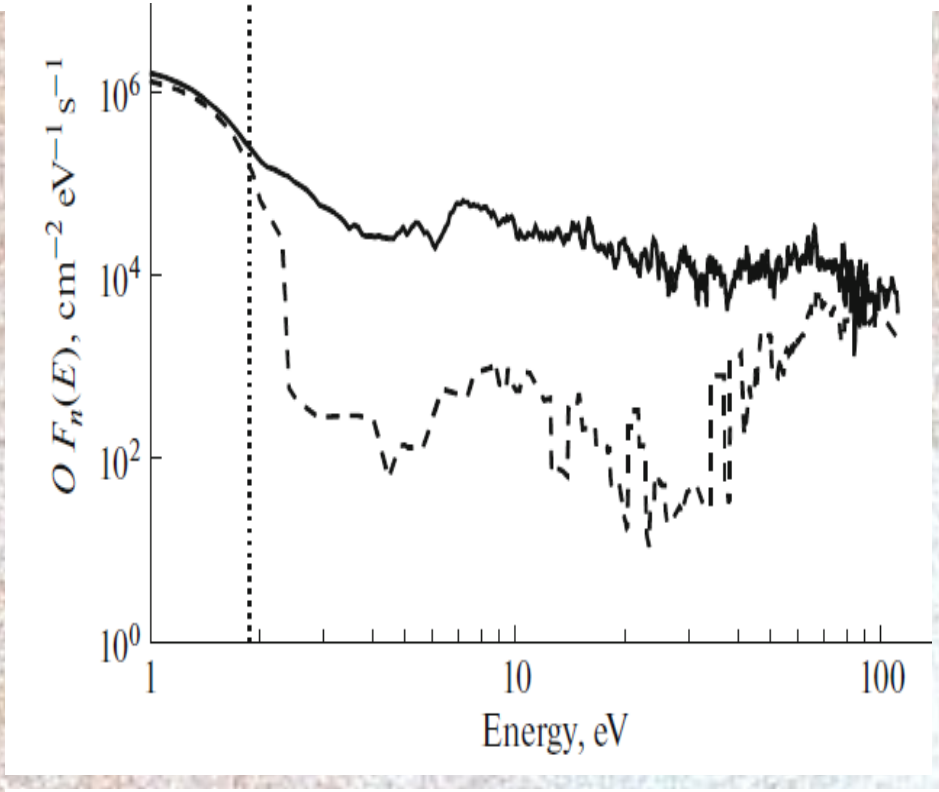

The calculated upward (solid lines) and downward (dashed lines) fluxes of suprathermal oxygen atoms in the upper atmosphere of Mars at altitude 220 km (Shematovich, 2021). At the 220-km level is in the Martian exosphere, from where oxygen atoms with suprathermal energies escape.

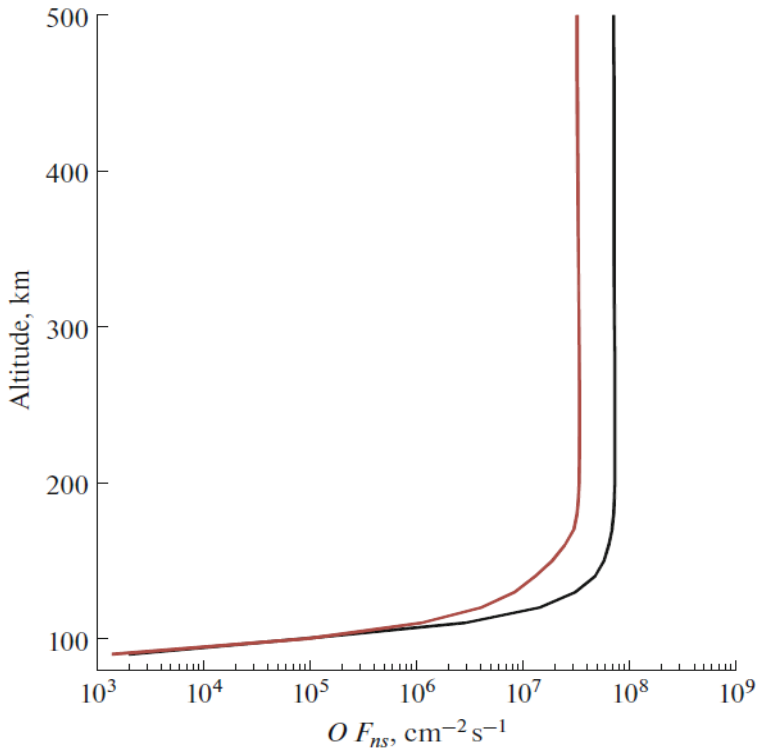

The altitude profiles for the upward flux of suprathermal oxygen atoms calculated for models A (black line) and B (brown line).

The escaping fluxes during the proton auroral events are equal to 5.8×10^7 cm^{-2}s^{-1} and 3.5×10^7cm^{-2}s^{-1} (Shematovich, 2021).

Proton auroral events at Mars - neutral O escape

Neutral O escaping flux due to the photochemistry is about (0.5 – 1.0)x10^{7} cm^{-2}s^{-1} depending on the solar activity level (Groeller et al., PSS, 2014).

Neutral O escaping flux due to the H^{+} and H precipitation is about (3.5 – 5.8)x10^{7} cm^{-2}s^{-1} for MAVEN/SWIA spectra of the precipitating protons for disturbed solar activity (Shematovich, 2021). These fluxes corespond to the global loss rates of (3.2-5.2)×10^{25} O s^{-1} .

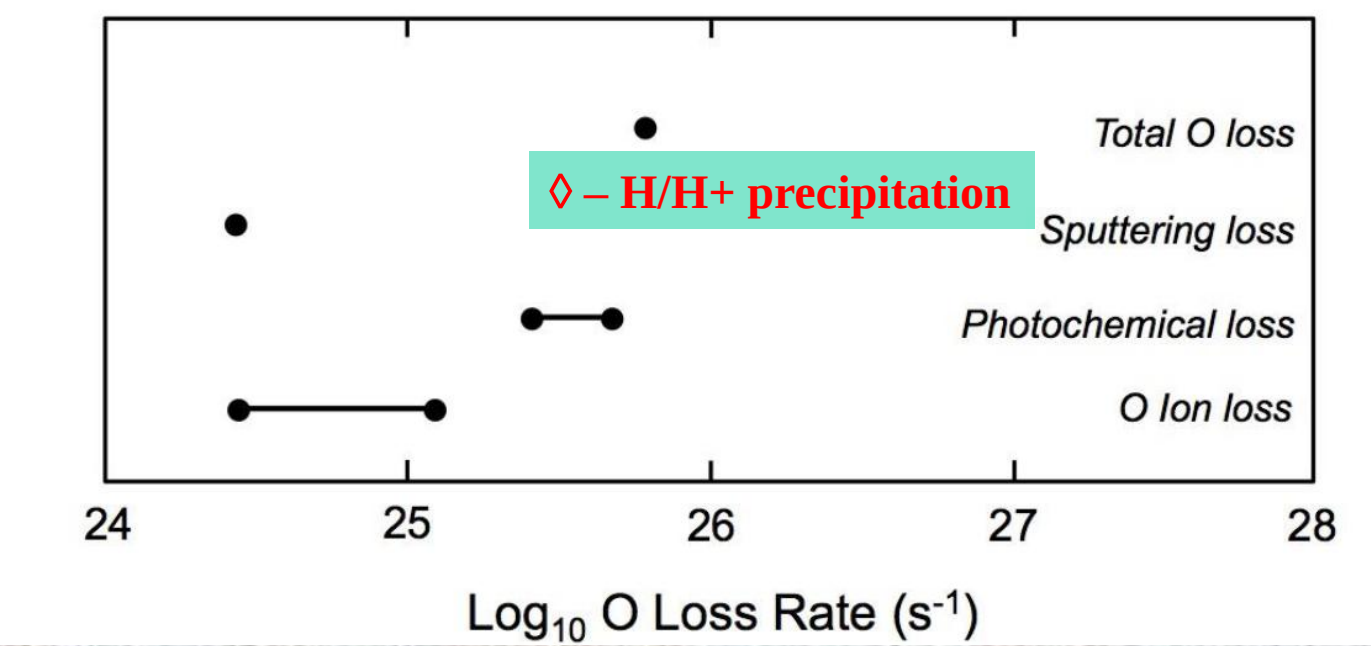

O loss rate as determined from MAVEN observations for each of the loss processes examined (Jakosky et al., Icarus, 2018).

MAVEN: *How much atmosphere has been lost at Mars?*

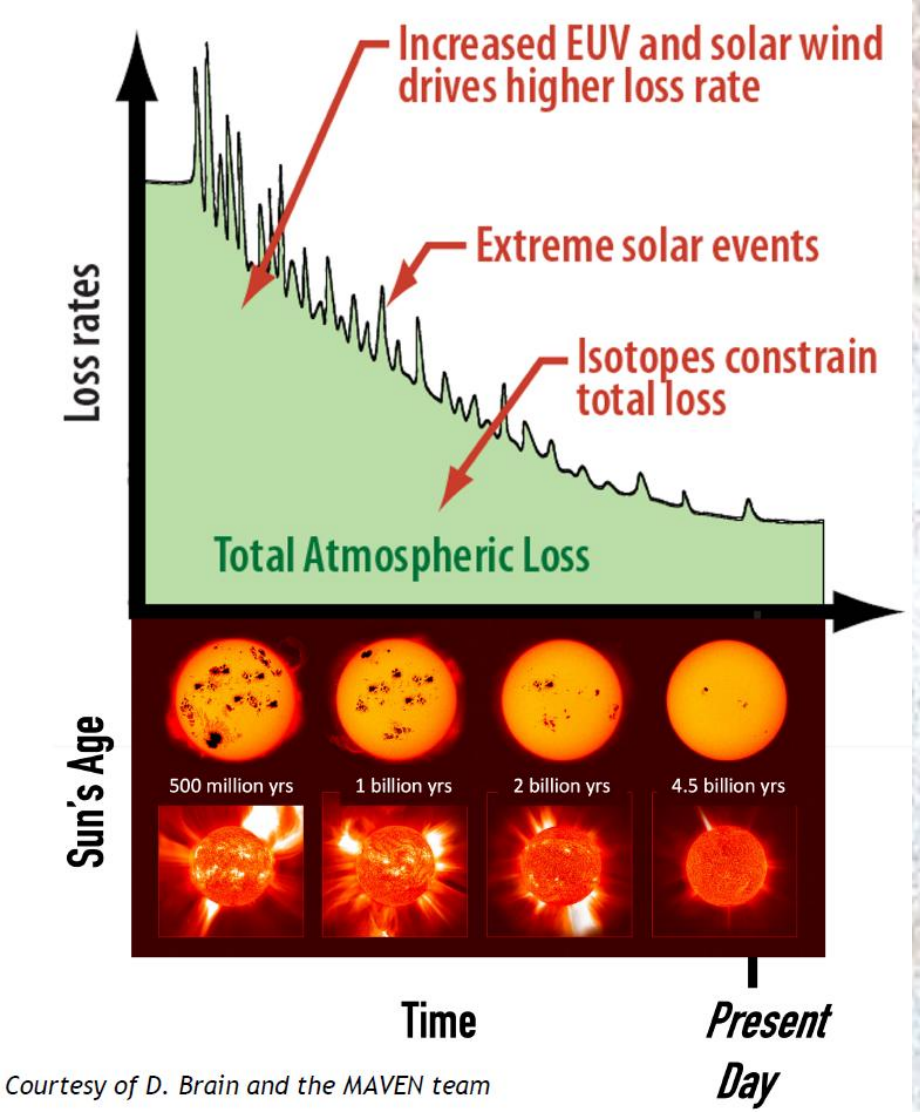

Courtesy of D. Brain and the MAVEN team

An *extrapolation back in time with current* escape rates, scaled to extreme rates during a more active sun, suggests that total escape rate would be responsible for the loss of a significant amount of water and/or atmosphere (Jakosky et al., 2018):

- **Current loss rate ~ 2-3 kg/s**
- **Mars would have lost with current LR:**

-H equivalent to a global water layer ~3.4 -24 m thick in 4 billion years;

-O equivalent to a global ~75 mbar CO_2 or ~2.3 m H_2O layer in 4 billion years.

- **Loss rates were changing in time because of the larger EUV solar flux, stronger solar wind and more abundant and intense solar storms for early Mars.**
- **Integrated O loss in the early Mars epoch of more than 0.8 bar of CO_2 or 23 m H_2O.**

HST Observations (Bhattacharyya et al., 2019, 2022): Modeling Thermal H with MAVEN-EUVM Temperatures

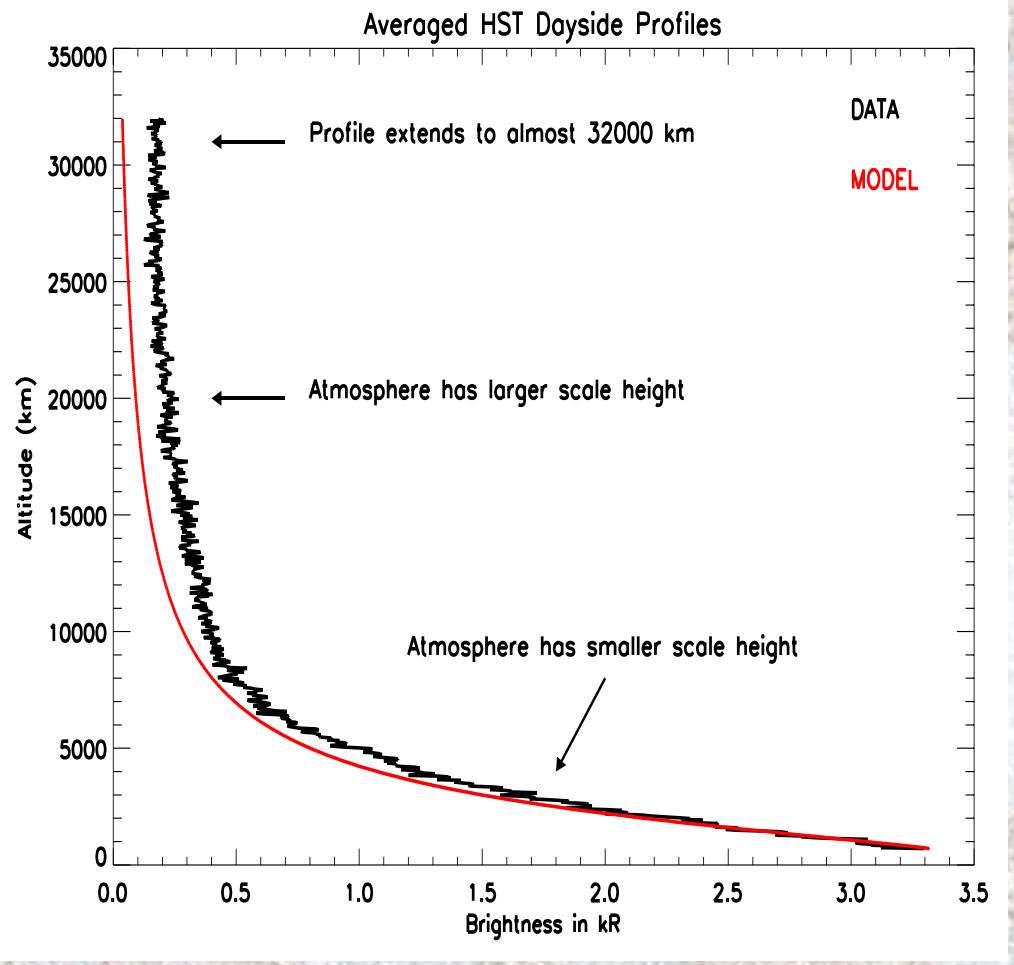

Thermal temperature was pre-determined through simulations of the MAVEN-EUVM data for the HST observation conditions.

Observation Date	Thermal H T_{exo} (K)	Thermal H N_{exo} (cm^{-3})
31st December 2017	271	42700 ± 2300
13th January 2018	218	68600 ± 8200
10th February 2018	190	83600 ± 5400

HST Observations (Bhattacharyya et al., 2019, 2022):
Kinetic MC Modeling of Hot H in the extended Martian H corona

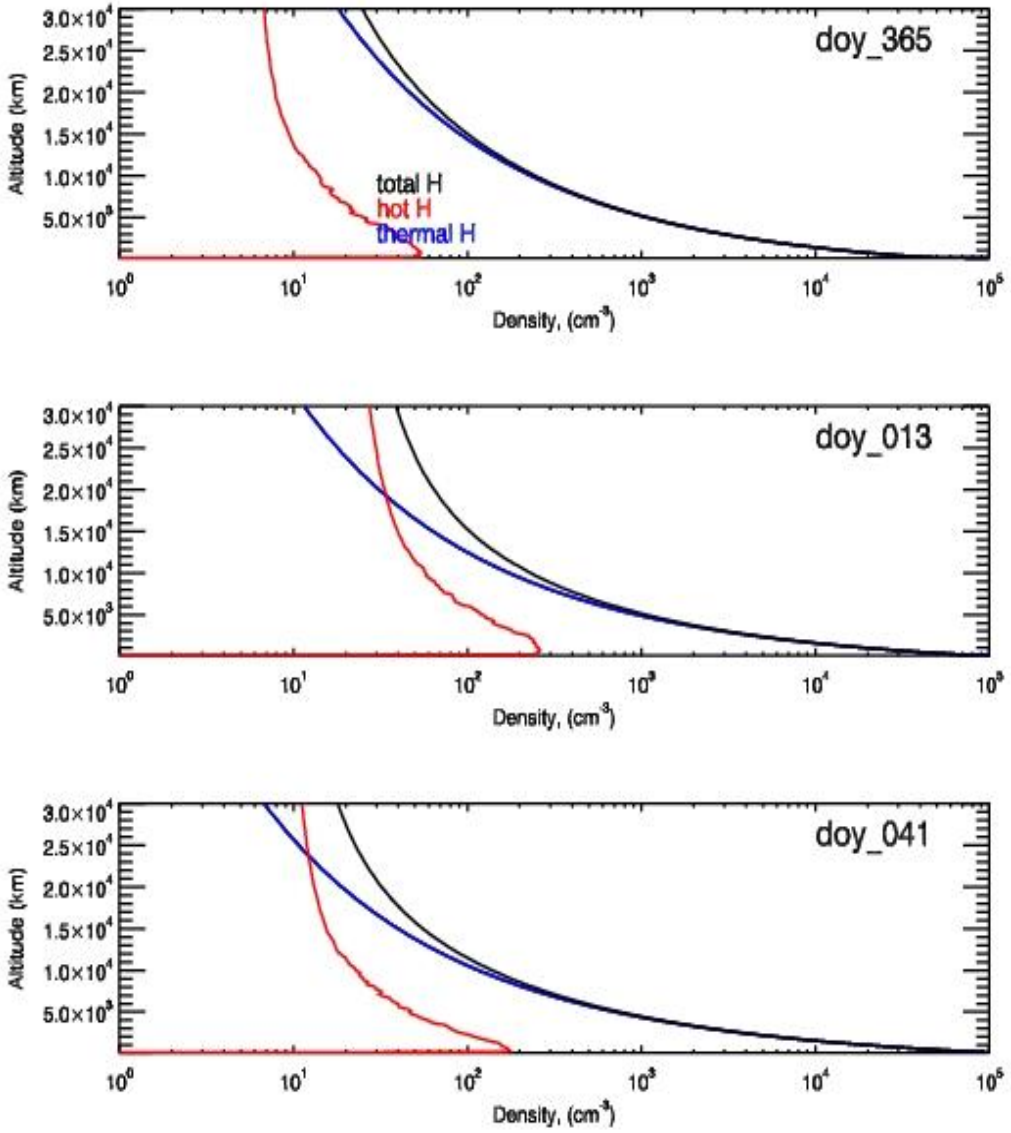

Kinetic Monte Carlo model of ENA-H precipitation (Shematovich et al., 2021) was used to calculate the distribution of hot H in the extended H corona at Mars.

Height profiles of the thermal (blue lines) and calculated hot (red lines) fractions of atomic hydrogen in the extended corona at Mars. Total H concentrations are shown by black lines.
Calculations were done for the dates:
-December 31, 2017 (upper panel), -January 13, 2018 (middle panel), and -February 10, 2018 (bottom panel)

when the HST observations of the hydrogen corona at Mars were made (Bhattacharyya et al., 2019, 2022). Hopefully, the calculated hot and thermal H height profiles will allow us to fit the HST observations (Bhattacharyya et al., 2019).

Conclusions: *hot atomic coronas at exoplanets*

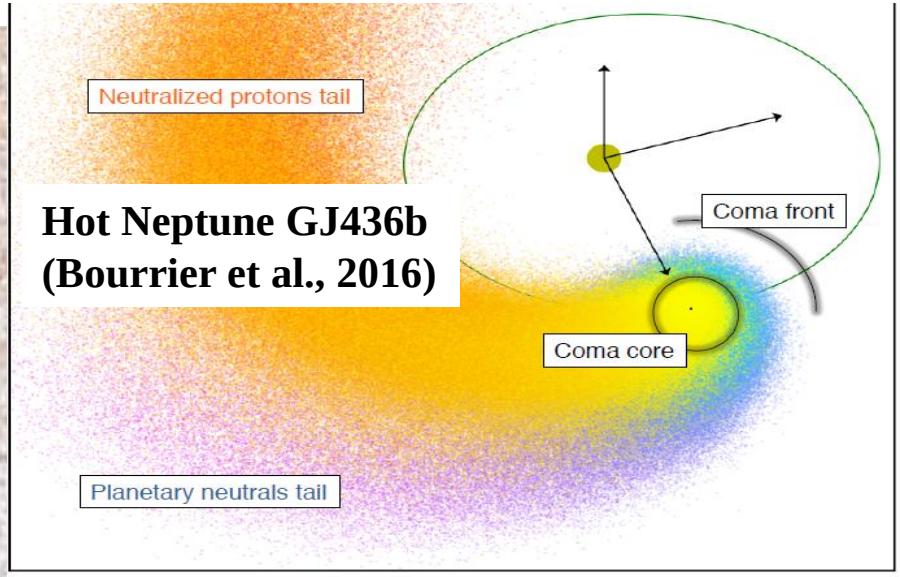

Hot Neptune GJ436b (Bourrier et al., 2016)

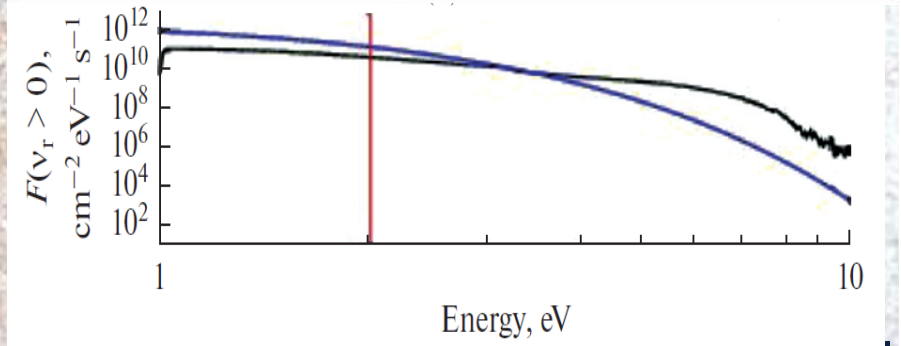

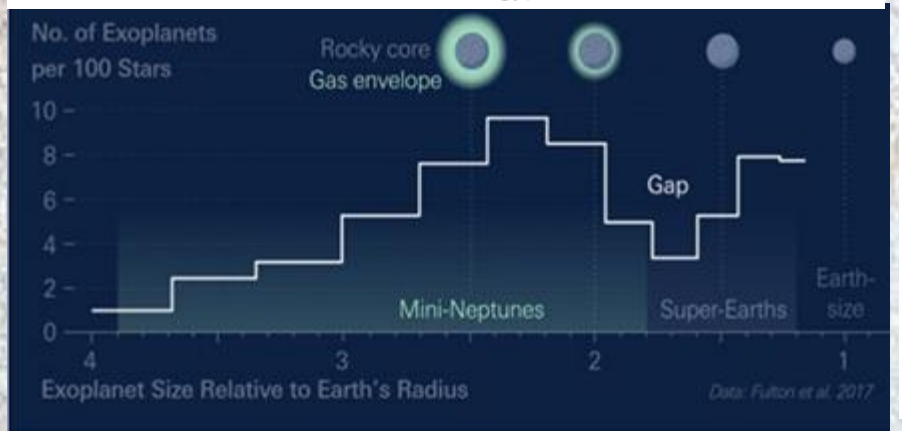

Hot atomic coronas at sub-, exo-, and super-Earths as well as at ocean planets and sub-Neptunes:

- **are formed due to both thermal and non-thermal processes induced by the stellar forcing on the planetary atmosphere;**
- **their structure strongly depend on the exoplanet orbit with more extended coronas for close-in exoplanets;**
- **oxygen corona can be observed for different types – H2O, O2, N2-O2, CO2, - of the surrounding atmosphere;**
- **UV observations of oxygen coronas could provide an important information on atmospheric biosignatures – O2, O3 and NO, N2O, - if the exoplanet is placed in the potential habitable zone of the host star.**

THANK YOU FOR YOUR ATTENTION!